Infiltration of Water Molecules into the Oseltamivir-Binding Site of H274Y Neuraminidase Mutant Causes Resistance to Oseltamivir

Jin Woo Park and Won Ho Jo*

Department of Materials Science and Engineering, Seoul National University, Seoul 151-742, Korea

Received September 16, 2009

The oseltamivir-resistant neuraminidase mutant, His274Tyr (H274Y), has recently been identified in humans. The objective of our present research is to elucidate the origin of resistance of the H274Y mutation to oseltamivir (OTV) at the molecular level via molecular dynamics simulation. For this purpose, the binding free energies of OTV with the wild-type N1 subtype and with the H274Y mutant were calculated using the linear interaction energy method. The nonbonded interaction energies between OTV and active-site residues were also calculated to investigate the contribution of nonbonded interactions to the total binding free energy. Our molecular dynamics trajectories revealed marked differences between these two structures, particularly in the binding modes of OTV. Contrary to the existing prediction, a salt bridge between Glu276 and Arg224 was retained in the OTV-bound H274Y mutant throughout the simulation. This study reveals that water molecules can infiltrate into the binding site of the H274Y mutant, suggesting that the origin of H274Y resistance to OTV is caused by penetration of water molecules into the binding site and not by disruption of the Glu276-Arg224 salt bridge. These results will be useful for the rational design of neuraminidase inhibitors having high potency against known drug-resistant H5N1 mutants.

INTRODUCTION

Influenza virus has two surface glycoproteins, hemagglutinin (HA) and neuraminidase (NA). The HA protein plays a role in the binding to cellular receptors and in the fusion of viral and endosomal membranes. The NA protein cleaves terminal sialic acid (*N*-acetylneuraminic acid) from glycoconjugates found on the surface of host cells and facilitates the release of progeny viruses from infected cells. As the active site of NA is relatively well conserved, it has been a good target for structure-based drug design. One of the most prevalent NA inhibitors designed in this manner is oseltamivir (OTV), which prevents the release of newly replicated influenza virions from infected cells. However, influenza viruses can develop resistance to the OTV via point mutations in NA. The recent emergence of OTV-resistant strains has raised serious concerns about a global flu pandemic because of their potential lethality to humans. A recent mathematical modeling study simulated the spread of influenza and concluded that the drug-resistant mutant could reduce the benefits of antiviral drug measures during a pandemic.[1]

Substitution of the wild-type histidine residue with tyrosine at amino acid position 274 (H274Y) in NA confers high-level resistance to OTV in N1-subtype influenza viruses. Researchers have thought that the H274Y mutation makes the virus less viable and that the OTV resistance would be a minor, manageable problem.[2] However, the strain of flu resistant to OTV has been circulating in the world, and the reason why the H274Y mutation has no effect on its viability is still unclear. It has been reported that the H274Y mutation in the N1 subtype results in up to a 265-fold higher resistance to OTV compared with that of the wild-type virus.[3] OTV-resistant influenza A (H5N1) viruses with the H274Y mutation have been isolated from humans who were treated with OTV for avian influenza.[4,5] Because the resistance can emerge during OTV therapy despite early initiation of treatment with the recommended dose,[5] it is necessary to develop new antiviral agents to which OTV-resistant influenza viruses remain susceptible. Therefore, it is necessary to understand the mechanism of resistance to OTV.

Elucidating the mechanism of OTV resistance is a top priority in virology because OTV is currently the most efficacious and common option for treatment and prophylaxis of the influenza virus infection.[6] A possible mechanism for OTV resistance has been proposed.[7−10] Wang et al.[7] examined the effects of side-chain size at residue 274 on the sensitivity to OTV and found that replacement of His274 with bulkier residues reduced the sensitivity of the N1 subtype to OTV, whereas replacement with smaller residues enhanced the sensitivity or had no effect. They concluded that, in the H274Y mutant, the conformational change of Glu276 required for the binding of OTV would be restricted, thereby decreasing the binding affinity of OTV for the N1 subtype; this suggested that the bulkiness of the Tyr274 could be the primary factor mediating the observed resistance of N1 to OTV. Based on these experimental data, recent computational studies also examined the influence of the substitutions at His274 by both smaller and larger side-chain residues on the sensitivity of the N1 subtype to OTV.[8] When His274 was substituted by a larger side-group residue, such as Phe or Tyr, the calculated binding free energies (−8.69 and −8.84 kcal/mol for Phe and Tyr, respectively) was higher than that of the wild-type N1 (−9.57 kcal/mol), indicating that the sensitivity of the NA to OTV was reduced by substitution of His274 with a larger side-group residue. However, the computational study predicted a quite different

* Corresponding author. E-mail: whjpoly@ snu.ac.kr.

10.1021/ci900348n
Published on Web 12/03/2009

orientation for OTV relative to the subsequently determined crystal structure of the H274Y mutant bound to OTV.[3] Another recent computational study conducted a molecular dynamics (MD) simulation for OTV in complex with the wild-type N1 or with three mutants, H274Y, N294S, and E119G and estimated the binding free energies of all complexes using the molecular mechanics/Poisson−Boltzmann surface area method.[9] They also concluded that, in the H274Y mutant, the consequent alteration of the conformational change of Glu276 upon OTV binding is a key factor for drug resistance. Moscona[10] also suggested that Glu276 of NA must rotate and form a salt bridge with Arg224 to accommodate the hydrophobic side group (−$OCHEt_2$) of OTV, but H274Y mutation inhibits this rotation of Glu276, resulting in resistance to OTV. This proposed reorientation of Glu276 in the NA active site of the N1 subtype is based on the structure of OTV bound to the N9 subtype.[11] However, we found that the binding affinity of OTV to the H274Y mutant was reduced compared to the wild-type N1, although the salt bridge between Glu276 and Arg224 was well retained in the H274Y mutant, indicating that there is another mechanism for the OTV resistance of the H274Y mutant.

In the present study, we also focused on the H274Y mutant bound to OTV because the H274Y mutation is prominent in lethal H5N1 strains and in the currently circulating H1N1 strains.[5,12] For the purpose of identifying the mechanism for the resistance of N1 to OTV, we analyzed structure variations of OTV in terms of the torsion angles of OTV and the number of water molecules penetrating into the cavity as OTV is bound to the H274Y mutant. We discovered that water molecules penetrating into the binding site are correlated with the observed lower binding affinity of the H274Y mutant for OTV, while the salt bridge between Glu276 and Arg224 was retained in both the H274Y mutant and the wild-type N1.

METHODS

Setup of Simulation Systems. Two parallel MD simulations of the N1−OTV system were carried out, one with the wild-type N1 subtype and the other with an N1 carrying the H274Y mutation in NA. The starting structures of the wild-type N1 subtype and H274Y mutant were taken from PDB entries 2HU0 and 3CL0, respectively.[3,13] The 2HU0 structure has a single OTV molecule, and the 3CL0 structure has four OTV molecules in an NA tetramer. Each monomer was named A, B, C, and D in the H274Y mutant. A box of TIP3P waters[14] was added to solvate each system, and then the two systems were neutralized by adding both sodium and chloride ions using visual molecular dynamics (VMD).[15] Overall, the OTV-containing wild-type N1 and mutant systems contained 90 795 atoms and 92 285 atoms, respectively.

The atomic charges of OTV were collected from the supporting information of Masukawa's work.[16] All equilibrium bond lengths, bond angles, and dihedral angles for OTV were calculated using the DMol^3 program based on the density functional theory (DFT).[17] Electronic configurations of molecular systems were described by restricted double-numerical basis sets with polarization functions for nitrogen and oxygen and without polarization functions for carbon and hydrogen. The general gradient approximation correction was applied to the energy calculation with the exchange functional of Becke[18] and the correlation functional of Perdew and Wang.[19] The conductor-like screening model[20] implemented into DMol^3 was used for incorporating the solvent effect into the DFT calculation.[21] We used a dielectric constant of 78.4 for the water. The missing force field parameters for OTV were assigned based on existing similar molecules already parametrized.

Details of MD Simulations. Energy minimization and MD simulations were performed using the NAMD program[22] with the CHARMM27 parameter set.[23] The final structures were energy minimized for 30 000 steps by the conjugate gradient method. Subsequently, the structures were heated from 0 to 310 K during 25 ps and equilibrated at this final temperature during another 10 ns as an NPT ensemble, using the Nosé-Hoover method at 310 K and at a pressure of 1 atm. As the wild-type N1 system had a single OTV molecule bound to the active site of one monomer, the other three monomers were fixed from 0.5 to 10 ns to focus our computational efforts on the calculation of the binding free energy of OTV, whereas the H274Y mutant system was equilibrated without any restraints. Electrostatic interactions were computed with the particle mesh Ewald algorithm,[24] and Lennard-Jones interactions were truncated at 12 Å. A time step of 1 fs was used throughout, and the trajectories were sampled every 10 ps.

Calculation of Binding Free Energy (ΔG_{bind}). We calculated the binding free energy of the OTV using the linear interaction energy (LIE) method, which enabled us to estimate the binding free energy from MD simulations with substantially lower computational cost. This LIE approach was recently used to predict binding affinities in various models of receptors and ligands.[25,26] The LIE method assumes that the binding free energy can be extracted from simulations of the free and bound state of the ligand. This simple approach is regarded as a good alternative to the more computationally demanding free energy perturbation calculations.[27,28] The LIE equation optimized for NA inhibitors has been well investigated.[29] The equation used in these calculations is

$$\Delta G_{bind} = 0.122\Delta U_{elec} + 0.472\Delta U_{vdw} + 2.603$$

where ΔU_{elec} and ΔU_{vdw} are the differences in the averaged inhibitor−environment electrostatic and van der Waals energies, respectively, between the two simulations. Free ligand simulation was performed during 0.1 ns in the NPT ensemble and then 1.9 ns in the NVT ensemble, and snapshots were taken every 0.1 ps (see the Supporting Information).

RESULTS AND DISCUSSION

Simulation Stability. Two MD simulations were performed to compare the binding affinity of OTV to the wild-type N1 and the H274Y mutant. The root-mean-square deviation (rmsd) profiles of NA, excluding hydrogen atoms, were analyzed relative to the initial structure (Figure 1). The results indicated that both systems reached equilibrium because no significant rmsd change was found after 5 ns of the MD simulation. Thus, trajectories from 5 to 10 ns were collected to analyze the results of simulation.

Comparison of Calculated Binding Free Energy. Binding free energies of OTV in complex with the wild-type N1

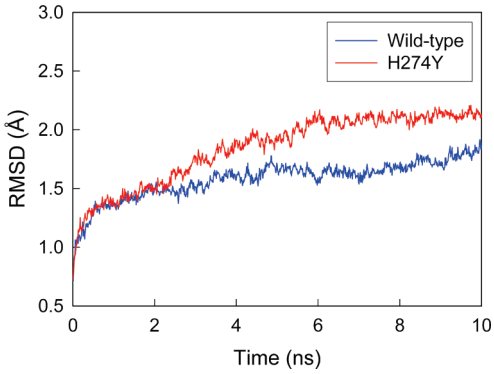

Figure 1. Rmsd profiles of the wild-type N1 (blue) and the H274Y mutant (red), except hydrogen atoms.

Table 1. Calculated Binding Free Energy (kcal/mol) of OTV for the Wild-type N1 and the H274Y Mutant[a]

NA	ΔU_{elec}[b]	ΔU_{vdw}[c]	ΔG_{bind}[d]
wild-type	−61.98 (1.47)	−11.33 (0.41)	−10.31 (0.37)
H274Y	−41.67 (1.38)	−11.40 (0.44)	−7.86 (0.38)

[a] Standard errors of the mean are given in parentheses. [b] Difference in electrostatic energy between bound and free states. [c] Difference in van der Waals energy between bound and free states. [d] Change of binding free energy.

and the H274Y mutant were separately calculated using the LIE method. For the wild-type N1, the calculated binding free energy of OTV is −10.31 kcal/mol (Table 1), in close agreement with the experimental value of −10.60 to −10.36 kcal/mol.[30] For the H274Y mutant, the calculated binding free energy is −7.86 kcal/mol. These results coincide with the fact that the H274Y mutant of the N1 subtype diminishes the binding affinity of OTV, resulting in OTV resistance. The difference between the two calculated binding free energies, 2.45 kcal/mol, is in good agreement with the experimental data[3] because the experimentally reported 265-fold decrease in OTV binding affinity upon H274Y mutation corresponds to the binding free energy differences ($\Delta\Delta G_{bind}$) of 2.99 kcal/mol at 310 K, where the standard thermodynamic relation, $\Delta G_{bind} = -RT \ln K_I$, where R, T, and K_I denote the gas constant, temperature, and inhibitory constant, respectively,[16,31] was used for estimation of the binding free energy. The low affinity of OTV to the H274Y mutant is mostly due to reduced electrostatic energy—the difference in electrostatic energies between two NA molecules ($\Delta\Delta U_{elec}$) is 20.31 kcal/mol, whereas that of van der Waals energies ($\Delta\Delta U_{vdw}$) is 0.07 kcal/mol.

To investigate the origin of the reduced electrostatic interaction of OTV in the H274Y mutant compared to the wild-type N1, we calculated nonbonded interaction energies between OTV and residues lining the binding site. The decomposition of interaction energies into contributions originating from different amino acid residues provides valuable information on the structure−activity relationship.[32,33] Figure 2 illustrates the electrostatic energies between OTV and residues in the H274Y mutant relative to the energy between OTV and residues in the wild-type N1. The OTV lost its favorable electrostatic interactions with Asp151, Arg152, Arg292, Ser179, Arg292, Asn294, Tyr347, and Arg371 in the H274Y mutant, while making other favorable interactions with Arg118, Glu119, Arg156, Glu227, Glu276, Glu277, and Tyr406. Among them, the interaction between

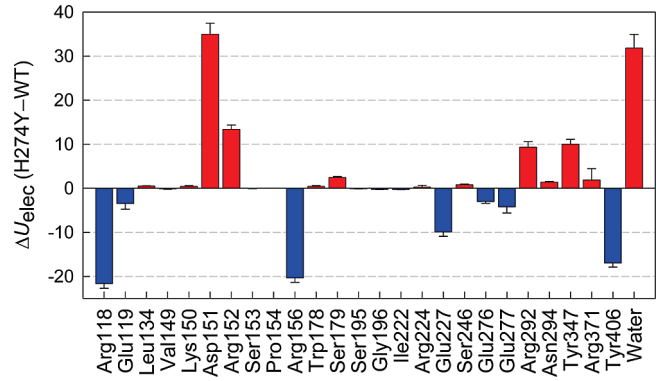

Figure 2. Electrostatic energies between OTV and the H274Y mutant relative to the energy between OTV and wild-type N1. Electrostatic energies of OTV with 25 neighboring amino acid residues were calculated as well as with water molecules. Positive values indicate that the electrostatic interaction between the OTV and the residue was reduced (red bars), whereas negative values represent increased interaction (blue bars) upon mutation. Error bars represent the standard error (95% confidence limits) of the mean.

OTV and Asp151 was most hindered by the H274Y mutation, indicating that the 150-loop of N1 opens upon mutation. Flexibility of the 150-loop has intensively been investigated by MD simulation studies,[34,35] which is also shown in our MD trajectories (see the Supporting Information). Interestingly, the results showed that the OTV interacts less favorably with water molecules in the H274Y mutant. These results suggest that water molecules play a critical role in the observed lower binding affinity of H274Y mutant for OTV.

Changes in the Structure of OTV. Comparison of the H274Y mutant and the wild-type N1 systems revealed a difference in OTV orientation. To investigate the effect of the mutation, changes in the molecular structure of OTV in the binding site were monitored in terms of torsion angles, ϕ_1−ϕ_6, defined by the following sets of four atoms, C7−C2−C1−O1B, C4−C5−N5−C10, C7−C6−O7−C8, C6−O7−C8−C9, O7−C8−C9−C91, and O7−C8−C81−C82, respectively (Figure 3A). The torsion angle of the $-COO^-$ side group of OTV, ϕ_1, is −120° in both the OTV-bound wild-type and H274Y structures, although ϕ_1 in the H274Y mutant has a broader torsion angle (Figure 3B). No significant differences in ϕ_2 for the −NHAc side group of OTV were found, as two sharp peaks appear at almost the same torsion angle, −120° (Figure 3C). These data show that the H274Y mutation does not have a significant influence on the orientation of the two side groups of OTV, namely $-COO^-$ and −NHAc.

Dramatic differences between the OTV-bound wild-type and the H274Y structures were observed in ϕ_3−ϕ_6 of OTV, however, indicating that the 1-ethylpropoxy group ($-OCHEt_2$) of OTV is sensitive to the H274Y mutation of N1. Angles ϕ_3 and ϕ_4 were rotated by 30° (from −120° to −90°) and by 60° (from 60° to 120°), respectively, as OTV is bound to the H274Y mutant, indicating that the C6−O7 bond is rotated toward the $-COO^-$ side group in the H274Y mutant (Figure 3D and E). The backward rotation of ϕ_4 in the H274Y mutant indicates that the $-OCHEt_2$ side group points away from the binding site. Interestingly, the ϕ_5 and ϕ_6 angles show more than one peak in the OTV−H274Y mutant system (Figure 3F and G). This indicates that the

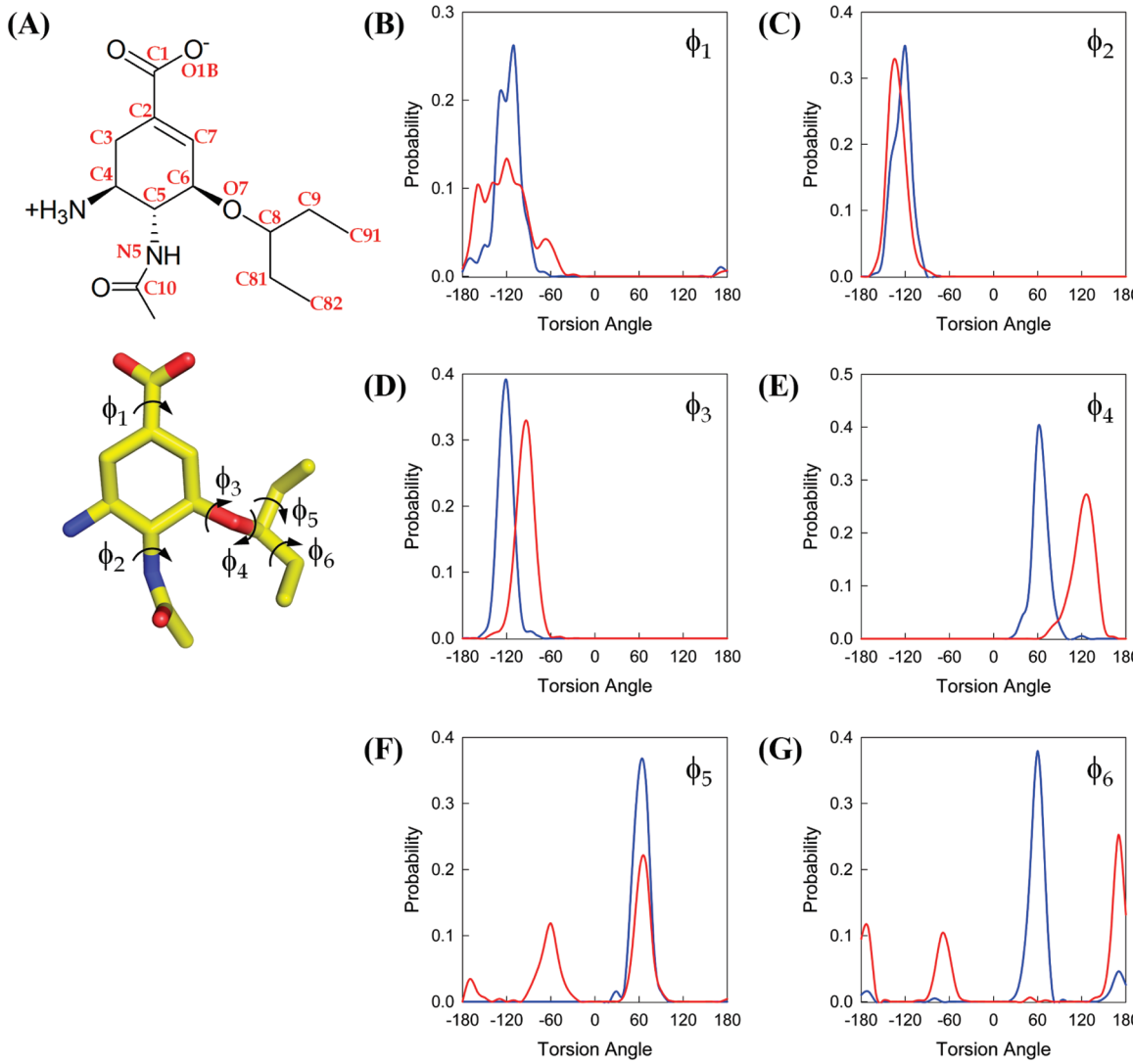

Figure 3. (A) Definition of OTV torsion angles, $\phi_1-\phi_6$. The atoms C, N, and O in OTV are colored by yellow, blue, and red, respectively. Hydrogen atoms were eliminated for clarity. (B−G) Distribution of torsion angles in the binding sites of the wild-type N1 (blue) and the H274Y mutant (red).

$-OCHEt_2$ side group of OTV undergoes greater fluctuation when bound to the H274Y mutant. Angle ϕ_5 in the H274Y mutant shows three peaks at 60°, −60°, and −170°, whereas ϕ_5 in the wild-type N1 shows only one peak at 60°. Angle ϕ_6 in the H274Y mutant also shows three peaks at 170°, −70°, and −170°, whereas ϕ_6 in the wild-type N1 shows two peaks at 60° and 170°. These results indicate a weaker interaction between the end of the $-OCHEt_2$ group and the neighboring residues in the H274Y binding site, implying that the $-OCHEt_2$ group of OTV is closely related to the resistance of the H274Y mutant to the OTV.

To further understand the importance of the $-OCHEt_2$ group in OTV resistance, the distances between the atoms of this group and the nearest residue, Glu276, were measured for the wild-type and H274Y systems (Figure 4). For this purpose, we selected an atom of Glu276, denoted by C_δ, as the reference atom. Atoms C9 and C91 were displaced 3−4 Å in the H274Y mutant compared to the displacement in the wild-type N1, whereas C8 and C81 were displaced approximately 2 Å. These results indicate that a small cavity is created in the OTV−H274Y mutant bound structure, perhaps allowing water molecules to intervene between the $-OCHEt_2$ group and the Glu276.

Infiltration of Water Molecules into the OTV-Binding Site. We monitored the number of water molecules that reside between the binding site and the OTV (Figure 5). Three virtual spheres of radius 6 Å were constructed by centering the atom C81 of OTV, C_δ of Glu276, and C_δ of Glu277, respectively; the water molecules that were detected within the areas where all three spheres overlapped were counted. The data show that water molecules exist in all H274Y monomers (A−D), whereas no water molecules were detected in the wild-type N1 throughout the simulation, as shown in Figure 5. In the wild-type N1, the $-OCHEt_2$ group of OTV binds deeper in the pocket, moving toward the floor in the direction of Glu276 (Figure 6A). In the H274Y mutant, Tyr274 forms hydrogen bonds with the amine group of Asn294 and with the carboxylate group of Glu276 (Figure 6B). Glu276 also forms a salt bridge with Arg224. The carboxyl oxygen atoms of Glu276 also serve as hydrogen-bond acceptors for two water molecules (which are themselves hydrogen bonded) and prevent the side group of OTV from penetrating as deeply into the H274Y pocket compared with that of the wild-type N1. It is noteworthy that a weaker, water-mediated interaction

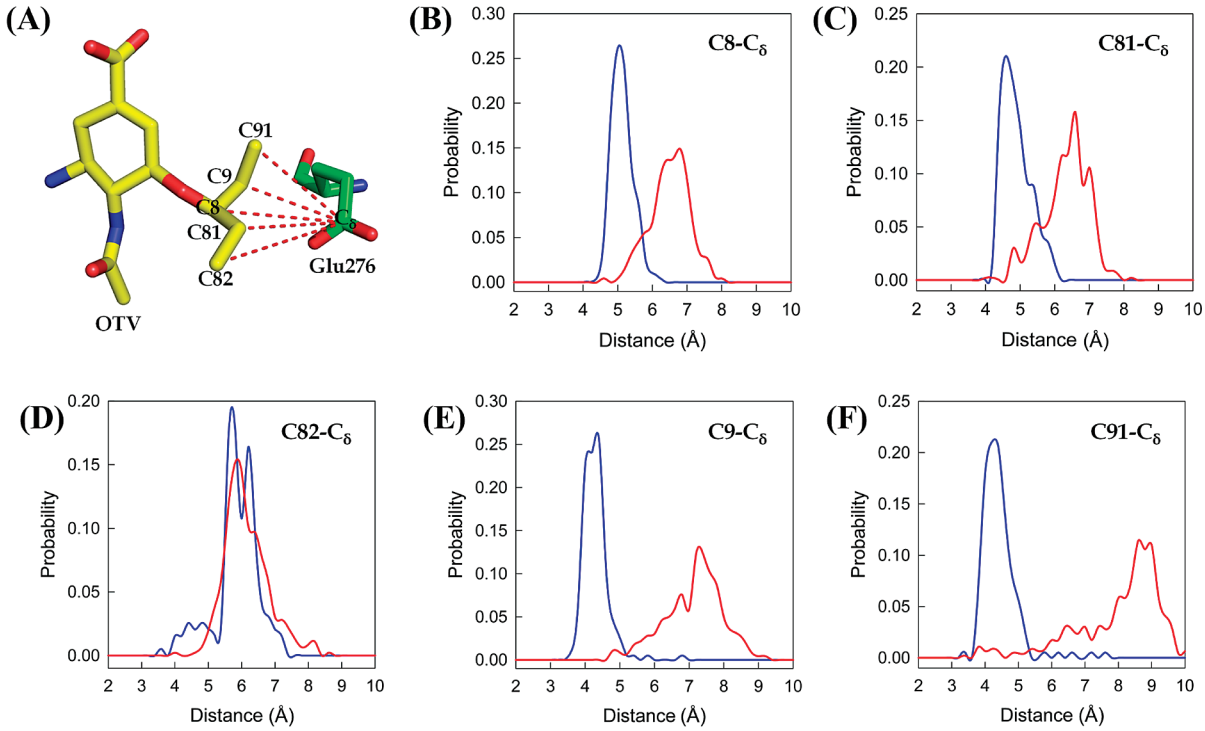

Figure 4. (A) OTV in the binding site and residue Glu276 are represented. The color representation is the same as in Figure 3. Carbon atoms of NA are depicted in green. (B−F) Distribution of distance between the C_δ atom of Glu276 and atoms: (B) C8, (C) C81, (D) C82, (E) C9, and (F) C91 of OTV in the wild-type N1 (blue) and the H274Y mutant (red) systems.

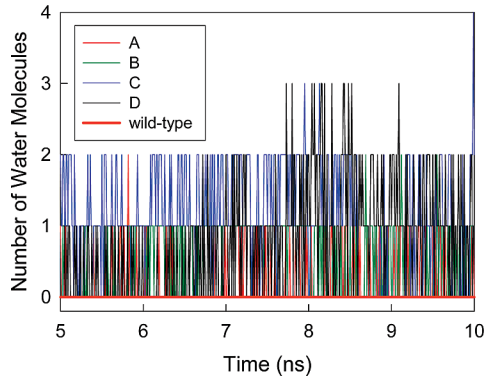

Figure 5. Number of water molecules percolating through the binding pocket in the wild-type N1 (thick red line) and the H274Y mutant (thin lines) systems. Three virtual spheres of radius 6 Å were constructed by centering the C81 atom of OTV, the C_δ atom of Glu276, and the C_δ atom of Glu277; water molecules that were detected within the areas where all three spheres overlapped were counted.

between OTV and mutant R292K NA has also been discovered in a group-two neuraminidase (H3N2).[11]

To confirm whether it is thermodynamically stable for water molecules to reside between the OTV and the binding site of the H274Y mutant, additional MD simulations were carried out for 3 ns. In the final structure of the H274Y mutant system, all water molecules residing in the cavity were manually moved 20 Å in the *z*-direction. For energy minimization, both NA and OTV were initially fixed to allow for relaxation of water molecules and ions, and then the energy minimization was continued without restraints. The initial 1 ns MD run was conducted with all water molecules fixed to prevent them from entering the binding site, and the following MD run was performed for 2 ns without restraints. The result showed that the total energy (the sum of the potential and the kinetic energies) of the system increased from −159 431 to −158 873 kcal/mol when water molecules were removed from the binding site, indicating that it is reasonable for water molecules to percolate through the gap.

Salt Bridge between Glu276 and Arg224. It has been proposed that a salt bridge between Glu276 and Arg224 is

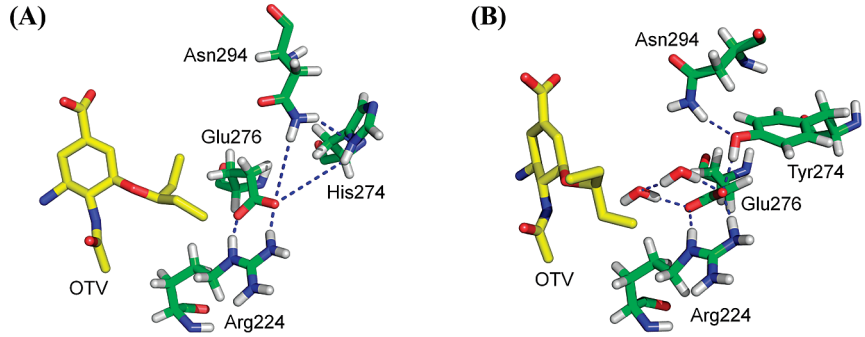

Figure 6. Snapshots of the binding site of (A) the wild-type N1 and (B) the H274Y mutant. Hydrogen bonds are shown as blue dashed lines. The atoms C, N, O, and H are colored by yellow (green in NA), blue, red, and gray, respectively. Hydrogen atoms of OTV were eliminated for clarity. Dramatic conformational change in $-OCHEt_2$ group of OTV are represented, also shown in Figures 3 and 4.

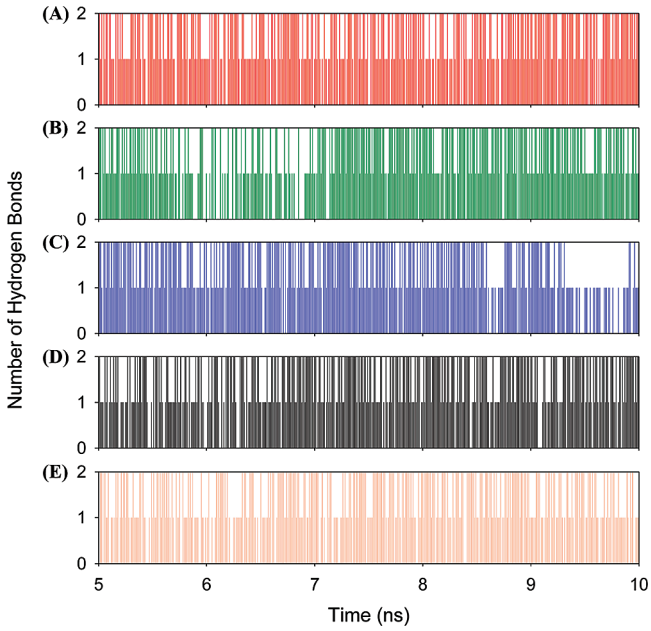

Figure 7. (A−D) Number of hydrogen bonds between Glu276 and Arg224 of the H274Y mutant in four monomers, respectively, and (E) the wild-type N1 during MD simulations. In this analysis, the hydrogen bond is defined by the following criteria: Donor and acceptor must be within 3 Å, and the angle formed by the donor, hydrogen, and acceptor must be larger than 160°.

an important part of the mechanism for OTV resistance because OTV had been expected to fail to induce the salt bridge formation between Glu276 and Arg224 in the H274Y mutant system.[3,10,11] The recently determined crystal structure of the H274Y mutant in complex with OTV has shown that the carboxyl group of Glu276 is shifted by 2.0 Å toward the binding pocket due to substitution of His274 with the bulkier Tyr residue.[3] However, our simulation results showed that the salt bridge was maintained since the OTV-H274Y mutant complex had reached an equilibrium state.

We next assessed the salt bridge formation during our simulation by identifying hydrogen bonds between Glu276 and Arg224 (Figure 7). For the entire simulation time, the hydrogen bond between Glu276 and Arg224 was stable in the H274Y mutant system (Figure 7A−D), with the guanidinium group of Arg224 functioning as a hydrogen-bond donor to the carboxyl oxygen atoms of Glu276 (∼87% occurrence). The fact that the salt bridge between Glu276 and Arg224 was retained for 87% of the time in the H274Y mutant indicates that the orientation of Glu276 is not the main factor underlying the resistance to OTV. Rather, our results suggest that the presence of water molecules in the OTV binding site induces the resistance of the H274Y mutant to the OTV.

CONCLUSIONS

To gain mechanistic insight into the molecular basis for resistance of influenza H5N1 to oseltamivir (OTV), we carried out all-atom molecular dynamic (MD) simulations of the N1 subtype bound to the OTV in both the wild-type NA and the H274Y mutant. We have confirmed that OTV binds to the H274Y mutant with lower affinity compared to the wild-type N1 by calculating the binding free energy. The simulation revealed that water molecules can infiltrate between the OTV and the binding site, resulting in the low binding affinity of OTV for the H274Y mutant. Contrary to the existing paradigm, the salt bridge between Glu276 and Arg224 in the H274Y mutant was maintained upon OTV binding. The binding affinity of OTV for NA seems to be more dependent on the interaction with active-site residues rather than on the reorientation of Glu276, which has also been reported in the literature.[8] Consequently, we suggest that the origin of resistance of the H274Y mutant to OTV is not the result of breakage of the salt bridge between Glu276 and Arg224 but more likely is caused by penetration of water molecules into the binding site.

ACKNOWLEDGMENT

This research was supported by WCU (World Class University) program (Hybrid Materials major, Seoul National University) through National Research Foundation of Korea funded by the Ministry of Education, Science and Technology.

Supporting Information Available: The 150-loop motions from MD simulation. Nonbonded interaction energy between oseltamivir and water molecules in the free ligand simulation. This material is available free of charge via the Internet at http://pubs.acs.org.

REFERENCES AND NOTES

(1) Lipsitch, M.; Cohen, T.; Murray, M.; Levin, B. R. Antiviral resistance and the control of pandemic influenza. *PLoS Med.* **2007**, *4*, 111–121.
(2) Enserink, M. A 'wimpy' flu strain mysteriously turns scary. *Science* **2009**, *323*, 1162–1163.
(3) Collins, P. J.; Haire, L. F.; Lin, Y. P.; Liu, J. F.; Russell, R. J.; Walker, P. A.; Skehel, J. J.; Martin, S. R.; Hay, A. J.; Gamblin, S. J. Crystal structures of oseltamivir-resistant influenza virus neuraminidase mutants. *Nature* **2008**, *453*, 1258–1261.
(4) Le, Q. M.; Kiso, M.; Someya, K.; Sakai, Y. T.; Nguyen, T. H.; Nguyen, K. H. L.; Pham, N. D.; Ngyen, H. H.; Yamada, S.; Muramoto, Y.; Horimoto, T.; Takada, A.; Goto, H.; Suzuki, T.; Suzuki, Y.; Kawaoka, Y. Avian flu - Isolation of drug-resistant H5N1 virus. *Nature* **2005**, *437*, 1108–1108.
(5) de Jong, M. D.; Thanh, T. T.; Khanh, T. H.; Hien, V. M.; Smith, G. J. D.; Chau, N. V.; Cam, B. V.; Qui, P. T.; Ha, D. Q.; Guan, Y.; Peiris, J. S. M.; Hien, T. T.; Farrar, J. Brief report - Oseltamivir resistance during treatment of influenza A (H5N1) infection. *New Engl. J. Med.* **2005**, *353*, 2667–2672.
(6) Moscona, A. Medical management of influenza infection. *Annu. Rev. Med.* **2008**, *59*, 397–413.
(7) Wang, M. Z.; Tai, C. Y.; Mendel, D. B. Mechanism by which mutations at His274 alter sensitivity of influenza a virus N1 neuraminidase to oseltamivir carboxylate and zanamivir. *Antimicrob. Agents Chemother.* **2002**, *46*, 3809–3816.
(8) Mihajlovic, M. L.; Mitrasinovic, P. M. Another look at the molecular mechanism of the resistance of H5N1 influenza A virus neuraminidase (NA) to oseltamivir (OTV). *Biophys. Chem.* **2008**, *136*, 152–158.
(9) Wang, N. X.; Zheng, J. J. Computational studies of H5N1 influenza virus resistance to oseltamivir. *Protein Sci.* **2009**, *18*, 707–715.
(10) Moscona, A. Oseltamivir resistance - Disabling our influenza defenses. *New Engl. J. Med.* **2005**, *353*, 2633–2636.
(11) Varghese, J. N.; Smith, P. W.; Sollis, S. L.; Blick, T. J.; Sahasrabudhe, A.; McKimm-Breschkin, J. L.; Colman, P. M. Drug design against a shifting target: a structural basis for resistance to inhibitors in a variant of influenza virus neuraminidase. *Structure* **1998**, *6*, 735–746.
(12) Ives, J. A. L.; Carr, J. A.; Mendel, D. B.; Tai, C. Y.; Lambkin, R.; Kelly, L.; Oxford, J. S.; Hayden, F. G.; Roberts, N. A. The H274Y mutation in the influenza A/H1N1 neuraminidase active site following oseltamivir phosphate treatment leave virus severely compromised both in vitro and in vivo. *Antiviral Res.* **2002**, *55*, 307–317.
(13) Russell, R. J.; Haire, L. F.; Stevens, D. J.; Collins, P. J.; Lin, Y. P.; Blackburn, G. M.; Hay, A. J.; Gamblin, S. J.; Skehel, J. J. The structure of H5N1 avian influenza neuraminidase suggests new opportunities for drug design. *Nature* **2006**, *443*, 45–49.

(14) Jorgensen, W. L.; Chandrasekhar, J.; Madura, J. D.; Impey, R. W.; Klein, M. L. Comparison of simple potential functions for simulating liquid water. *J. Chem. Phys.* **1983**, *79*, 926–935.
(15) Humphrey, W.; Dalke, A.; Schulten, K. VMD: Visual molecular dynamics. *J. Mol. Graphics* **1996**, *14*, 33–38.
(16) Masukawa, K. M.; Kollman, P. A.; Kuntz, I. D. Investigation of neuraminidase-substrate recognition using molecular dynamics and free energy calculations. *J. Med. Chem.* **2003**, *46*, 5628–5637.
(17) Delley, B. Analytic energy derivatives in the numerical local-density-functional approach. *J. Chem. Phys.* **1991**, *94*, 7245–7250.
(18) Becke, A. D. Density-functional exchange-energy approximation with correct asymptotic behavior. *Phys. Rev. A: At., Mol., Opt. Phys.* **1988**, *38*, 3098–3100.
(19) Perdew, J. P.; Wang, Y. Accurate and simple analytic representation of the electron-gas correlation energy. *Phys. Rev. B: Condens. Matter* **1992**, *45*, 13244–13249.
(20) Klamt, A.; Schuurmann, G. COSMO-A new approach to dielectric screening in solvents with explicit expressions for the screening energy and its gradient. *J. Chem. Soc., Perkin Trans. 2* **1993**, 799–805.
(21) Yang, S. H.; Huh, J.; Jo, W. H. Effect of solvent polarity on the initiation and the propagation of ethylene polymerization with constrained geometry catalyst/MAO catalytic system: A density functional study with the conductor-like screening model. *Macromolecules* **2005**, *38*, 1402–1409.
(22) Kale, L.; Skeel, R.; Bhandarkar, M.; Brunner, R.; Gursoy, A.; Krawetz, N.; Phillips, J.; Shinozaki, A.; Varadarajan, K.; Schulten, K. NAMD2: Greater scalability for parallel molecular dynamics. *J. Comput. Phys.* **1999**, *151*, 283–312.
(23) Brooks, B. R.; Bruccoleri, R. E.; Olafson, B. D.; States, D. J.; Swaminathan, S.; Karplus, M. CHARMM: A program for macromolecular energy, minimization, and dynamics calculations. *J. Comput. Chem.* **1983**, *4*, 187–217.
(24) Darden, T.; York, D.; Pedersen, L. Particle mesh Ewald: An $N\cdot\log(N)$ method for Ewald sums in large systems. *J. Chem. Phys.* **1993**, *98*, 10089–10092.
(25) Stjernschantz, E.; Marelius, J.; Medina, C.; Jacobsson, M.; Vermeulen, N. P. E.; Oostenbrink, C. Are automated molecular dynamics simulations and binding free energy calculations realistic tools in lead optimization? An evaluation of the linear interaction energy (LIE) method. *J. Chem. Inf. Model.* **2006**, *46*, 1972–1983.
(26) Perdih, A.; Bren, U.; Solmajer, T. Binding free energy calculations of N-sulphonyl-glutamic acid inhibitors of MurD ligase. *J. Mol. Model.* **2009**, *15*, 983–996.
(27) Alonso, H.; Bliznyuk, A. A.; Gready, J. E. Combining docking and molecular dynamic simulations in drug design. *Med. Res. Rev.* **2006**, *26*, 531–568.
(28) Bren, U.; Martinek, V.; Florian, J. Free energy simulations of uncatalyzed DNA replication fidelity: Structure and stability of T center dot G and dTTP center dot G terminal DNA mismatches flanked by a single dangling nucleotide. *J. Phys. Chem. B* **2006**, *110*, 10557–10566.
(29) Wall, I. D.; Leach, A. R.; Salt, D. W.; Ford, M. G.; Essex, J. W. Binding constants of neuraminidase inhibitors: An investigation of the linear interaction energy method. *J. Med. Chem.* **1999**, *42*, 5142–5152.
(30) Govorkova, E. A.; Leneva, I. A.; Goloubeva, O. G.; Bush, K.; Webster, R. G. Comparison of efficacies of RWJ-270201, zanamivir, and oseltamivir against H5N1, H9N2, and other avian influenza viruses. *Antimicrob. Agents Chemother.* **2001**, *45*, 2723–2732.
(31) Brown, K. L.; Bren, U.; Stone, M. P.; Guengerich, F. P. Inherent Stereospecificity in the Reaction of Aflatoxin B-1 8,9-Epoxide with Deoxyguanosine and Efficiency of DNA Catalysis. *Chem. Res. Toxicol.* **2009**, *22*, 913–917.
(32) Bren, U.; Martinek, V.; Florian, J. Decomposition of the solvation free energies of deoxyribonucleoside triphosphates using the free energy perturbation method. *J. Phys. Chem. B* **2006**, *110*, 12782–12788.
(33) Bren, M.; Florian, J.; Mavri, J.; Bren, U. Do all pieces make a whole? Thiele cumulants and the free energy decomposition. *Theor. Chem. Acc.* **2007**, *117*, 535–540.
(34) Amaro, R. E.; Minh, D. D. L.; Cheng, L. S.; Lindstrom, W. M.; Olson, A. J.; Lin, J. H.; Li, W. W.; McCammon, J. A. Remarkable loop flexibility in avian influenza N1 and its implications for antiviral drug design. *J. Am. Chem. Soc.* **2007**, *129*, 7764–7765.
(35) Udommaneethanakit, T.; Rungrotmongkol, T.; Bren, U.; Frecer, V.; Stanislav, M. Dynamic Behavior of Avian Influenza A Virus Neuraminidase Subtype H5N1 in Complex with Oseltamivir, Zanamivir, Peramivir, and Their Phosphonate Analogues. *J. Chem. Inf. Model.* **2009**, *49*, 2323–2332.

CI900348N